arXiv:1401.6515v1 [cond-mat.mtrl-sci] 25 Jan 2014

Spin-Orbit Interaction Effects in the Electronic Structure of B20-type CoSi: First-Principles Density Functional Study

Fumiyuki ISHII[1], Hiroki KOTAKA[2], and Takashi ONISHI[2]

[1]*Faculty of Mathematics and Physics, Kanazawa University, Kanazawa, 920-1192, Japan*
[2]*Graduate School of Natural Science and Technology, Kanazawa University, Kanazawa, 920-1192, Japan*

E-mail: fishii@mail.kanazawa-u.ac.jp

(Received October 20, 2013)

We have performed fully relativistic first-principles density functional calculations for non-magnetic B20-type CoSi. The spin-orbit interaction has crucial effects on the electronic structures of a chiral crystal. The calculated band structure around the Fermi energy shows Bloch vector k-linear dispersion expressed by a *real-spin* Weyl Hamiltonian, i.e., a mass-less Dirac Hamiltonian. We found the hedgehog-like spin textures in Bloch $\boldsymbol{k}$-vector space (momentum space) on the isoenergy surface around the Γ point. The Fermi velocity for k-linear dispersion is about $0.22v_F^g$, where v_F^g is the Fermi velocity of graphene.

KEYWORDS: Spin-orbit interaction, Weyl point, Dirac cone, Spin texture, First-principles calculation

1. Introduction

B20-type monosilicides, such as MSi (M:transition metal), are known to show anomalous electrical and magnetic properties at low temperatures; examples include a Kondo insulator in FeSi [1] and a helical spin structure in MnSi [2] and $Fe_{1-x}Co_xSi$ [3]. The helical magnetic structures are thought to be due to a lack of an inversion center in its crystal structure. Then, the Dzyaloshinskii-Moriya interactions [4, 5] are induced by a relativistic spin-orbit interaction (SOI) effect. Recently, the spin-vortex, skyrmion-lattice phase was discovered in the B20-type monosilicides [6, 7] and the peculiar spin textures are expected to be applicable for spintronics applications [8].

In addition to the relativistic SOI effect on the spin textures in *real space*, there also exist relativistic SOI effects on the spin textures in the *momentum space*. In nonmagnetic systems, with time-reversal symmetry, the breaking of the inversion symmetry of the crystal has a crucial effect on the electronic structures. In general, the eigenenergies depends on the Bloch-states vector $\boldsymbol{k}$ and spin vector $\boldsymbol{\sigma}$. There is a relationship between the energies due to the time-reversal symmetry $E(\boldsymbol{k}, \boldsymbol{\sigma}) = E(-\boldsymbol{k}, -\boldsymbol{\sigma})$, as well as the space inversion symmetry $E(\boldsymbol{k}, \boldsymbol{\sigma}) = E(-\boldsymbol{k}, \boldsymbol{\sigma})$. Therefore, if the system has both symmetries, the electronic states at every $\boldsymbol{k}$-point has doubly degenerate eigenenergies, as $E(\boldsymbol{k}, \boldsymbol{\sigma}) = E(\boldsymbol{k}, -\boldsymbol{\sigma})$. On the other hand, if the system does not have space inversion symmetry, the eigenenergies have spin splitting, i.e., $E(\boldsymbol{k}, \boldsymbol{\sigma}) \neq E(\boldsymbol{k}, -\boldsymbol{\sigma})$, except for the time-reversal invariant $\boldsymbol{k}$-points, $\boldsymbol{k} = 0, \boldsymbol{G}_i/2$, where $\boldsymbol{G}_i (i = 1, 2, 3)$ is the reciprocal lattice vector.

This spin-splitting is known for the structural inversion asymmetry (SIA) induced SOI effect. The Rashba effect [9] and Dresselhaus effect [10] are well known for polar semiconductors and their heterostructures. The $\boldsymbol{k}$-dependent spin Hamiltonian in noncentrosymmetric superconductors [11–13] and spin textures on the surface of materials [14, 15] have been extensively studied in this context. Recently, the SIA-induced SOI effect has attracted much attention because it induces the current-driven spin transfer torque [16]. Although there have been several studies on the electronic

structures of CoSi [17–19], the SOI effect has not been considered.

In this paper, we have performed fully relativistic first-principles density functional calculations for B20-type CoSi and discussed the effect of SOI in the electronic structure. Using noncollinear spin-density functional theory implemented in OPENMX code [20], we investigated the spin texture and electronic states. We found that the spin-splitting k-linear band structures, Dirac cone bands, can be expressed by a *real-spin* Weyl Hamiltonian, i.e., $H_{eff} = v_F(k_x\sigma_x + k_y\sigma_y + k_z\sigma_z)$, where v_F denotes the Fermi velocity. The Dirac cone bands in CoSi originate from the B20 structure, chiral space group $P2_13$. As reported in a previous study, Dirac cone bands already exist in the scalar-relativistic (without SOI) band structure of CoSi [18]. Such spin-degenerated Dirac cone bands are expressed by a *pseudo-spin* Weyl Hamiltonian, i.e., *pseudo-spin* mass-less Dirac Hamiltonian often discussed in the graphene. Recently, the group theoretical derivation of a *pseudo-spin* Weyl Hamiltonian for some space group has been reported [21]. Contrary to the *pseudo-spin* Weyl Hamiltonian, those of the *real-spin* discussed in this paper are quite important for spin-dependent phenomena, as stated before.

2. Methods

Using the OPENMX code [20], we performed fully relativistic first-principles electronic-structure calculations based on density functional theory (DFT) within the generalized gradient approximation (GGA) [22]. The norm-conserving pseudopotential method [23] was used. We used a linear combination of multiple pseudo atomic orbitals generated by a confinement scheme [24, 25]. We used an (8,8,8) uniform k-point mesh. The pseudo atomic orbitals were expanded as follows: Co5.5-s3p3d3f1 and Si5.5-s3p3d1. The spin textures were calculated by post-processing calculation after the self-consistent field potential was obtained, as in our previous study [26]. We calculated the $\boldsymbol{k}$-space spin density matrix $P_{\sigma,\sigma'}(\boldsymbol{k},\mu)$ using the spinor wave-function whose component is given by $\Psi_\sigma(\boldsymbol{r},\boldsymbol{k},\mu)$, obtained from the self-consistent calculations as follows: $P_{\sigma,\sigma'}(\boldsymbol{k},\mu) = \int d\boldsymbol{r}\Psi^*_\sigma(\boldsymbol{r},\boldsymbol{k},\mu)\Psi_{\sigma'}(\boldsymbol{r},\boldsymbol{k},\mu)$, where μ is the band index and σ and σ' are the spin indexes ($\uparrow,\downarrow$), respectively. We deduced the spin polarization in the $\boldsymbol{k}$-space from the 2×2 spin density matrix. Because the wave function $\Psi_\sigma(\boldsymbol{r},\boldsymbol{k},\mu)$ is given by a linear combination of pseudo atomic orbitals, we can decompose the calculated spin polarization to its atomic components. The crystal structure we used in this study is the experimental lattice constant and internal parameters: a=4.444Å, $x_{\rm Co}$=0.143, $x_{\rm Si}$=0.844, for CoSi [27]. In addition to the (x,x,x), there are three equivalent sites, 3 permutations of (x+1/2, 1/2-x, $-x$). Therefore, there are 8 atoms in the unitcell.

3. Results and Discussions

Figure 1 shows the calculated electronic band structure of CoSi. Figure 1(a) shows a wide energy range covering 2 eV above/below the Fermi energy ($E_{\rm F}$). The calculated band structure of CoSi is similar to that of scalar-relativistic (without SOI) one [18], as well as those of B20-type FeSi [28], MnSi [29, 30] and CoGe [31]. Around the $E_{\rm F}$ and Γ point, there are two types of characteristic dispersion bands. One is the Dirac cone-like k-linear dispersing bands (Dirac cone bands). The other one is much less dispersing bands (flat bands). These characteristic band structures around the E_F, composed of the Dirac cone bands and the flat bands, are considered to be the origin for the large Seebeck coefficient [18, 31].

Next, we focused on the spin splitting around the E_F. In particular, we are interested in the Dirac cone bands; we plotted the band structure around the $E_{\rm F}$ on the $-{\rm M}(-0.5,-0.5,0)-\Gamma(0,0,0)-{\rm M}(0.5,0.5,0)$ symmetry line, as shown in Fig. 1 (b). The spin splitting of the bands can be seen, except for the Γ point due to the SIA-induced SOI effect mentioned above. Here, we speculate the symmetry character of the bands at the Γ-point around the $E_{\rm F}$ based on the known double group

character table [32]. Without considering SOI, the $E_{\rm F}$ lies at the spin degenerate orbital triplet state Γ_4. Because of the SOI, the 6-fold degenerate Γ_4 is split into a lower-energy doublet and two higher-energy doublets. In other words, around below the $E_{\rm F}$ at the Γ-point, there is a Γ_5 doublet. Γ_6 and Γ_7, two degenerate doublets, are above the $E_{\rm F}$. The spin-orbit splitting of CoSi at the Γ point is about 54.6 meV. The Dirac cone bands cross above the $E_{\rm F}$. Then the so-called Weyl point is in the degenerate doublets, Γ_6 and Γ_7.

We evaluated the Fermi velocity of the Dirac cone bands. The obtained Fermi velocity for one of the Dirac cone bands, the higher energy band, is about 0.195 $\times 10^6$ m/s, which is about 22$\%$ that of graphene, 0.885 $\times 10^6$ m/s. To proceed with the analysis of the Dirac cone bands, we extracted the Dirac cone band as shown in Fig. 2(a). We also plotted the calculated spin polarization $\boldsymbol{P}$(P$_x$, P$_y$, P$_z$) as a vector arrow on the bands. Because the $-{\rm M}-\Gamma-{\rm M}$ line lies in the k_xk_y plane, we projected the P_x and P_y component on the line (horizontal axis) and plotted the P_z component on the vertical axis. The horizontal arrows in Fig. 2 (a) mean that there is no P_z component. This result is consistent with the Dirac cone bands expressed by the *real-spin* Weyl Hamiltonian, i.e., $H_{eff} = v_F(k_x\sigma_x + k_y\sigma_y + k_z\sigma_z)$.

Figure 2 (b) shows the band structure around the Γ-point above the Weyl point. There are two bands; one band is the linear dispersing Dirac cone band, and the other is a relatively parabolic band. The parabolic band is connected to the flat band below the band crossing point. Here, we are interested in the differences in the magnitude of spin polarization between the Dirac cone band and parabolic band. As seen in Fig. 2(b), the magnitude of the spin polarization of the parabolic band decreases when it is close to the degenerate point. On the other hand, as seen in Fig. 2(a) and (b), the magnitude of the spin polarization in the Dirac cone band is almost constant. The magnitude of the spin polarization of the Dirac cone band is twice as large as that of the parabolic band for the states at 0.06 eV above the $E_{\rm F}$, as shown in Fig. 2 (c). We decomposed the spin polarization to the atomic components. As a result, at states 0.06 eV above the $E_{\rm F}$, the spin polarization consists of more than 80 percent Co orbitals for both Dirac cone and parabolic bands.

We show the hedgehog-like spin texture on the isoenergy for 0.2 eV above the Fermi energy in Fig. 3. The spin texture of the lower-energy parabolic dispersion shows spin directed from the Γ point outwards, as shown in Fig. 3(a). On the other hands, the spin texture of the higher-energy linear dispersion shows spin directed towards the Γ point, as shown in Fig. 3(b). These results indicate that both the Dirac cone bands and parabolic bands are expressed by the *real-spin* Weyl Hamiltonian.

The origin of hedgehog-like spin texture is the chiral crystal structure. Space group P2$_1$3 does not have mirror symmetry, so the spin Hamiltonian, which is linear in k, will have a nonzero $k_i\sigma_i (i = x, y, z)$ term. If we have m_{xy} mirror symmetry where the mirror plane lies in the xy plane, the polar vector $\boldsymbol{k}(k_x, k_y, k_z)$ is transformed to $(k_x, k_y, -k_z)$ and the axial vector $\boldsymbol{\sigma}(\sigma_x, \sigma_y, \sigma_z)$ is transformed to $(-\sigma_x, -\sigma_y, \sigma_z)$. Then, the $k_i\sigma_i (i = x, y, z)$ terms disappear in the non-chiral crystal structure. There are twelve symmetry operations in space group P2$_1$3, $\{$E, 4C$_3$, 4C$_3^2$, 3C$_2$ $\}$. We can derive the Weyl Hamiltonian from the rotational invariant condition for the Hamiltonian. Thus, in space group P2$_1$3, $k_i\sigma_i (i = x, y, z)$ terms only remain in the Hamiltonian. The spin Hamiltonian can also be derived from group theory [11, 14, 15, 33]. Our derivation of the spin Hamiltonian is simpler than those given in previous studies.

4. Summary

We have performed fully relativistic first-principles density functional calculations for non-magnetic B20-type CoSi with SOI. The calculated band structures around the Fermi energy show k-linear dispersion expressed by a real-spin Weyl Hamiltonian, i.e., mass-less Dirac Hamiltonian. We found the hedgehog-like spin textures in momentum space on the isoenergy surface around the Γ point. The Fermi velocity for the linear dispersion is about $0.22v_F^g$, where v_F^g is the Fermi velocity of

graphene. Our findings provide the basis for the further studies on noncentrosymmetric superconductivity [12, 13] and spin related transport properties [34, 35] in B20-type materials.

Acknowledgements

The authors thank the Yukawa Institute for Theoretical Physics at Kyoto University. Discussions during the YITP workshop YITP-W-13-01 on "Dirac electrons in solids" were useful to complete this work. Part of this research has been funded by the MEXT HPCI Strategic Program. This work was partly supported by Grants-in-Aid for Scientific Research (Nos. 25104714, 25790007, and 25390008) from the JSPS. The computations in this research were performed using the supercomputers at the ISSP, the University of Tokyo.

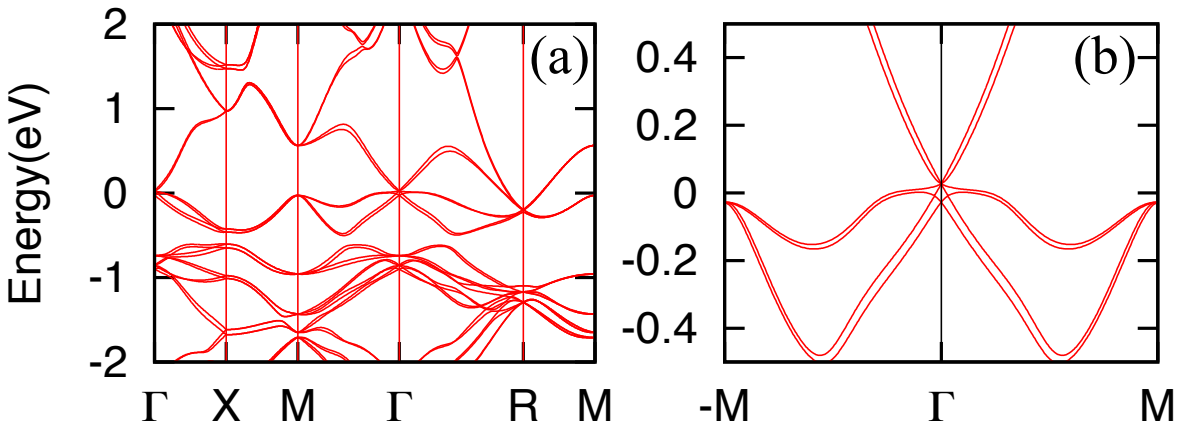

Fig. 1. (Color online) Fully relativistic calculated band structure of CoSi, a wide energy range covering 2 eV above/below the Fermi energy (a) and around the Fermi energy (b). The origin of the energy is taken at the Fermi energy. The high-symmetry $\boldsymbol{k}$-point symbols in the first Brillouin zone are denoted as Γ(0,0,0), X(0.5,0,0), M(0.5,0.5,0), R(0.5,0.5,0.5), -M(-0.5,-0,5,0) by the $\frac{\pi}{a}$ unit.

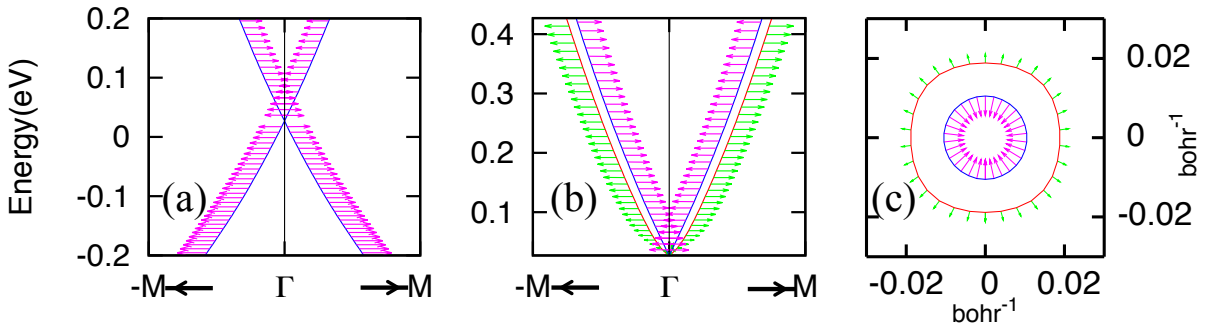

Fig. 2. (Color online) Fully relativistic calculated band structure around the Γ point for CoSi with calculated spin polarization. (a) The band structure of the extracted k-linear dispersion, (b) the band structure above the Weyl point. (c) The isoenergy (0.06eV) line with calculated spin polarization on $k_x - k_y$ plane ($k_z = 0$).

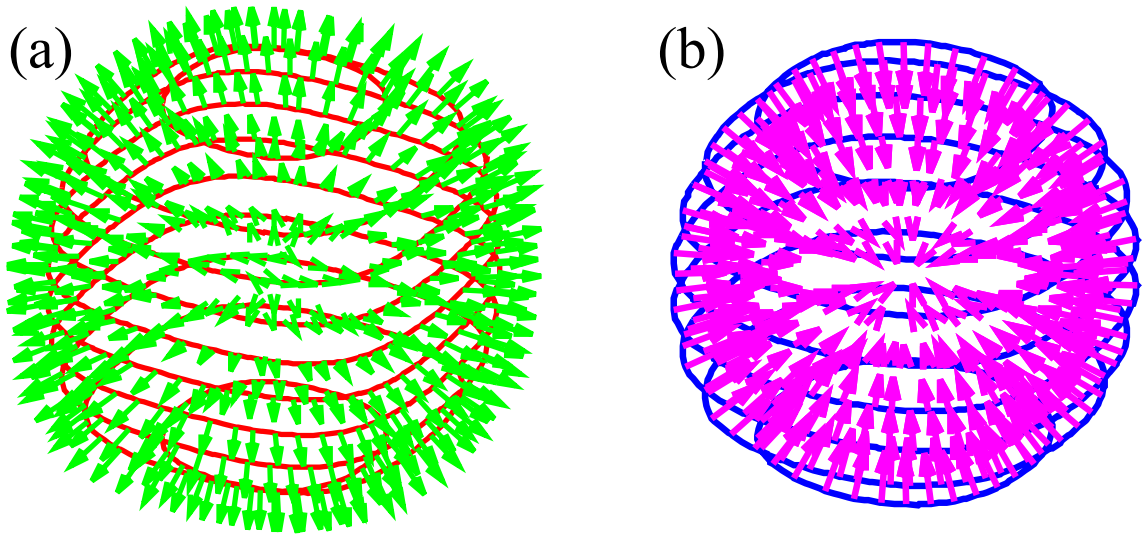

Fig. 3. (Color online) Calculated spin polarization on the isoenergy surface for 0.2eV above the Fermi energy for (a) the parabolic band and (b) the Dirac cone band.

References

[1] L. Degiorgi: Rev. Mod. Phys. **71** (1999) 687.
[2] G. Shirane, R. Cowley, C. Majkrzak, J. Sokoloff, B. Pagonis, C. Perry, and Y. Ishikawa: Phys. Rev. B **28** (1983) 6251.
[3] K. Ishimoto, Y. Yamaguchi, S. Mitsuda, M. Ishida, and Y. Endoh: J. Magn. Magn. Mater. **54** (1986) 1003.
[4] I. Dzyaloshinsky: J. Phys. Chem. Solids **4** (1958) 241.
[5] T. Moriya: Phys. Rev. **120** (1960) 91.
[6] S. Muehlbauer, B. Binz, F. Jonietz, C. Pfleiderer, A. Rosch, A. Neubauer, R. Georgii, and P. Boeni: Science **323** (2009) 915.
[7] X. Z. Yu, Y. Onose, N. Kanazawa, J.-H. Park, J. H. Han, Y. Matsui, N. Nagaosa, and Y. Tokura: Nature **465** (2010) 901.
[8] F. Jonietz, S. Mühlbauer, C. Pfleiderer, A. Neubauer, W. Münzer, A. Bauer, T. Adams, R. Georgii, P. Böni, R. A. Duine, K. Everschor, M. Garst, and A. Rosch: Science **330** (2010) 1648.
[9] E. I. Rashba: Sov. Phys. Solid State **2** (1960) 1109.
[10] G. Dresselhaus: Phys. Rev. **100** (1955) 580.
[11] P. A. Frigeri: Doctoral and Habilitation Theses, ETH Zürich (2005).
[12] P. A. Frigeri, D. F. D. Agterberg, A. A. Koga, and M. M. Sigrist: Phys. Rev. Lett. **92** (2004) 097001.
[13] P. A. Frigeri, D. F. Agterberg, A. Koga, and M. Sigrist: Phys. Rev. Lett. **93** (2004) 99903.
[14] T. Oguchi and T. Shishidou: J. Phys.: Condens. Matter **21** (2009) 2001.
[15] S. Vajna, E. Simon, A. Szilva, K. Palotas, B. Ujfalussy, and L. Szunyogh: Phys. Rev. B **85** (2012) 75404.
[16] I. M. Miron, G. Gaudin, S. Auffret, B. Rodmacq, A. Schuhl, S. Pizzini, J. Vogel, and P. Gambardella: Nature Materials **9** (2010) 230.
[17] Y. Imai, M. Mukaida, K. Kobayashi, and T. Tsunoda: Intermetallics **9** (2001) 261.
[18] A. Sakai, F. Ishii, Y. Onose, Y. Tomioka, S. Yotsuhashi, H. Adachi, N. Nagaosa, and Y. Tokura: J. Phys. Soc. Jpn. **76** (2007) 093601.
[19] Y. V. Kudryavtsev, V. A. Oksenenko, Y. P. Lee, J. Y. Rhee, and Y. D. Kim: J. Appl. Phys. **102** (2007) 3503.
[20] T. Ozaki, H. Kino, J. Yu, M. J. Han, M. Ohfuti, F. Ishii, K. Sawada, Y. Kubota, T. Ohwaki, H. Weng, M. Toyoda, H. Kawai, Y. Okuno, R. Perez, P. P. Bell, T. Duy, Y. Xiao, A. M. Ito, and K. Terakura: Available from: (http://www.openmx-square.org/) .
[21] J. L. Mañes: Phys. Rev. B **85** (2012) 155118.

[22] J. P. Perdew, K. Burke, and M. Ernzerhof: Phys. Rev. Lett. **77** (1996) 3865.
[23] N. Troullier and J. L. Martins: Phys. Rev. B **43** (1991) 1993.
[24] T. Ozaki: Phys. Rev. B **67** (2003) 155108.
[25] T. Ozaki and H. Kino: Phys. Rev. B **69** (2004) 195113.
[26] H. Kotaka, F. Ishii, and M. Saito: Jpn. J. App. Phys. **52** (2013) 5204.
[27] J. Teyssier, R. Viennois, J. Salamin, E. Giannini, and D. Van Der Marel: J. Alloys Compd. **465** (2008) 462.
[28] L. F. Mattheiss and D. R. Hamann: Phys. Rev. B **47** (1993) 78100.
[29] O. Nakanishi, A. Yanase, and A. Hasegawa: J. Magn. Magn. Mater. **15** (1980) 879.
[30] T. Jeong and W. E. Pickett: Phys. Rev. B **70** (2004) 075114.
[31] N. Kanazawa, Y. Onose, Y. Shiomi, S. Ishiwata, and Y. Tokura: Appl. Phys. Lett. **100** (2012) 3902.
[32] C. J. Bradley and A. P. Cracknell: *The mathematical theory of symmetry in solids* (Clarendon Press, Oxford, 2007).
[33] K. V. Samokhin: Ann. Phys. **324** (2009) 2385.
[34] H. Ohta, T. Arioka, E. Kulatov, S. Mitsudo, and M. Motokawa: J. Magn. Magn. Mater. **177** (1998) 1371.
[35] Y. Onose, N. Takeshita, C. Terakura, H. Takagi, and Y. Tokura: Phys. Rev. B **72** (2005) 224431.